



Original Paper

Deformation Characteristics and Mechanical Constitutive Model of Coal Under Stress Wave Action

Zhoujie Gu,^{1,2} Rongxi Shen,^{1,2,4} Siqing Zhang,^{1,2} Xin Zhou,^{1,2} Zhentang Liu,^{1,2}
Enlai Zhao,^{1,2} Xiulei Wang,^{1,2} and Jianbin Jia³

Received 13 April 2024; accepted 16 July 2024

The three-dimensional (3D) stress waves of coal samples were studied using a true triaxial split Hopkinson pressure bar compression rod. The results indicate that the 3D strain of the coal samples increased gradually under vibration load. The 3D stress wave of coal samples showed attenuation characteristics, and the change amplitude of the stress wave of coal samples along the direction of dynamic load was the most obvious. The amplitude of stress wave was the largest in the axial direction constrained by pre-stressing 3 MPa, while the amplitude of stress wave in the lateral 2 MPa pre-stressing was smaller than that under the constraint of 1 MPa. The results showed that the main deformation of coal samples was along the impact direction, while the larger horizontal and vertical lateral binding forces limited the deformation of coal samples. The Fourier transform was performed on the 3D stress wave of the coal samples, and the change in the amplitude of the stress wave spectrum was correlated positively with the vibration. The spectrum amplitude of the coal samples under the pre-stressed 3 MPa constraint (axial) direction was the largest, while the spectrum amplitude of the coal samples under the lateral 2 MPa pre-stressed constraint was smaller than that under the binding 1 MPa. However, the main frequency of the three-way stress wave was distributed in 0–10 kHz. By calculating the energy consumption rate and wave velocity decay rate, it was verified that the damage of coal samples increased with increase in dynamic load. This experimental testing provides an effective testing method for studying the 3D stress waves of coal samples under complex stress medium conditions. In addition, a dynamic constitutive model of coal was constructed according to the mechanical behavior of coal and rock mass and the measured data.

KEY WORDS: True triaxial, Stress wave, Strain, Damage, Constitutive model.

INTRODUCTION

Examining the durability and behavior of coal-like materials when subjected to vibration loading is crucial for defense and underground projects. For instance, vibrations from explosions and mining typically travel as stress waves through coal rock, impacting the nearby surroundings (Niu et al., 2020; Li et al., 2023d; Shen et al., 2024; Hu et al., 2024). Analyzing the way stress waves travel through coal rock bodies under both static and dynamic loads is

¹Key Laboratory of Gas and Fire Control for Coal Mines, Ministry of Education, China University of Mining & Technology, Xuzhou 221116, China.

²School of Safety Engineering, China University of Mining & Technology, Xuzhou 221116, China.

³Xinmi Hengye Co., Ltd, Zhengzhou 452376, China.

⁴To whom correspondence should be addressed; e-mail: shenrongxi@126.com

crucial for ensuring the dynamic stability of coal rock in underground working areas and evaluating the safety measures for underground engineering projects.

Ju et al. (2007) concluded that the attenuation of the stress wave is related to joints in rock, which indicated roughness. Li et al. (2011) constructed a fractal damage model based on related research. Feng et al. (2016) described the attenuation process of stress wave in coal by introducing the quality factor Q , and confirmed that the crack extension of a coal body under the action of stress wave is dominated by tensile cracks. Wang et al. (2018) found that the reflection coefficient is correlated negatively with the strain rate, while the transmission coefficient is correlated positively with the strain rate. Li et al. (2019) found that the larger the clip angle between rock bodies, the faster the attenuation of the stress wave. Yu et al. (2019) measured the average propagation velocity of stress waves in coral sand and proposed a dimensionless equation for the attenuation of peak stress with propagation distance. Huang et al. (2020) concluded that the transmittance coefficient of the stress wave of rock samples is correlated negatively with water pressure. Han et al. (2020, 2022) found that the reflection coefficient increases gradually and the transmission coefficient decreases with increase in thickness of mortar filling in rock samples. Kong et al. (2021) concluded that the transmittance wave of coal samples decreases with increase in axial pressure and gas pressure, and increases with increase in circumferential pressure and dynamic load (σ_d). Li et al. (2021) and others conducted dry ice cracking experiments at a field site and concluded that the attenuation of stress waves at a certain distance showed an inverse proportional function law. Wang et al. (2022a, 2022b) analyzed the effects of frequency, joints and wave impedance on the attenuation characteristics of rock stress waves. They used digital image correlation to analyze the stress wave attenuation process within the simultaneous length by testing the displacement field of granite during dynamic compression. Xie et al. (2022a, 2022b) innovatively used optical fiber to test and analyze the internal deformation characteristics of coal samples. Li et al. (2023e) found that the incident, reflected and transmitted wave of coal samples have attenuation processes after being subjected to dynamic loading, and the changes in the surface displacement of coal samples have a certain correlation with changes in the stress waves. Yang et al. (2023) analyzed that the stress wave attenuation ratio of rocks increases with the increase of temperature.

The above-mentioned previous tests of stress wave have focused on testing using Hopkinson compression rods, which are analyzed by capturing the stress wave signals from their incident and transmitted bar. Alternatively, stress wave signals can be obtained by attaching strain gauges at different locations on the rectangular sample. In some cases, stress wave signals generated by vibration or blasting can be collected at the base of the experimental site. All these test methods focus mainly on one-dimensional stress wave testing, whereas in this study, a true triaxial split Hopkinson pressure bar was used to apply a pre-determined circumferential pressure to the coal samples so as to test the three-directional stress waves of the samples, and their deformation characteristics and stress wave patterns were analyzed. In this study, the dynamic experiments of coal samples under different impact loads were carried out by applying three unequal pre-stresses of 3 MPa, 2 MPa and 1 MPa to coal samples. The stress waveforms in three directions of the coal samples were obtained, the strain in three directions was analyzed and the deformation characteristics of the coal samples were revealed. The stress wave changes of coal samples under different binding conditions were compared and analyzed, and the stress wave spectrum changes of coal samples in three directions were analyzed. The damage degrees of the coal samples were analyzed by calculating energy consumption rate and wave velocity test. Finally, considering the pre-stressed σ_1 , σ_2 and σ_3 of the coal samples, a mechanical constitutive model under true triaxial condition was constructed. This study provides useful reference for the study of three-way stress waves and deformation characteristics of coal samples.

EXPERIMENT

Experimental Equipment

Figure 1 shows the true triaxial split Hopkinson pressure bar rod experimental setup, which consisted mainly of a bullet launching device, an incident bar, a pre-stressing device and a transmitted bar, and signals can be collected by a hyperdynamic strain gauge through the strain gauges pasted on the incident and transmitted bar. The incident and transmissive bars as well as the strain gauges are attached to a sample are of type BX120-3AA, and the sensitive grids of the strain gauges are made of

Deformation Characteristics and Mechanical Constitutive Model

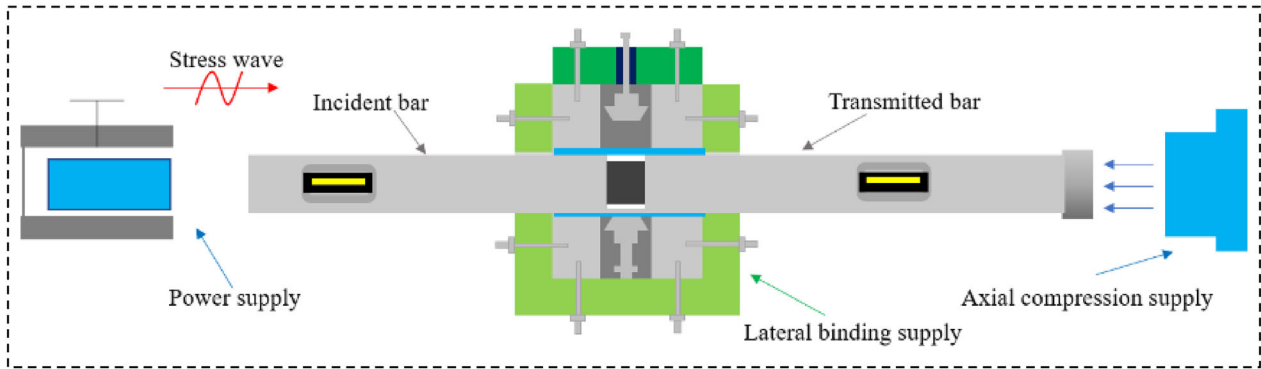
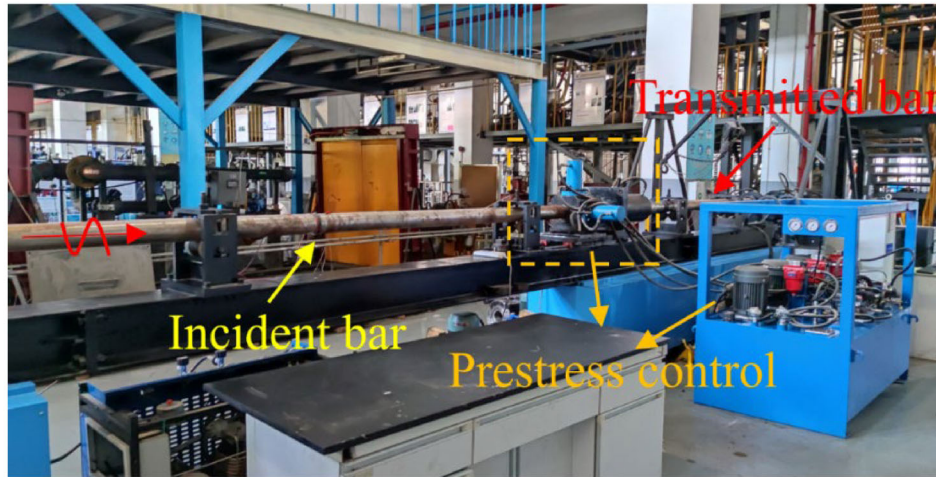


Figure 1. Schematic diagram of the true three-axis dynamic impact experimental device.

copper-chromium alloy. The pre-stressing device provides three static pre-stresses σ_1 , σ_2 and σ_3 , of varying or equal magnitudes to a sample. The maximum loading force of pre-stress can reach more than 60 MPa. Subsequently, the bullet launcher is activated to impact the projectile rod, creating a stress wave that acts on a sample, which is the source of σ_d on a sample. The corresponding sample can provide a maximum speed of up to 40 m/s. Additional description of this experimental equipment can be found in Gu et al. (2023a).

Figure 2 shows the coal samples used in this experiment. The coal for cutting the samples was selected from a mining area in Inner Mongolia, China. In order to prevent damage of the original state and structure of the coal samples, all the samples were processed with large chunks of coal as far as possible. The coal samples taken were sealed with soft plastic film and sent to the laboratory for

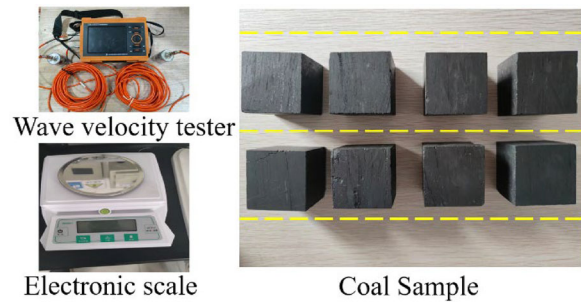


Figure 2. Coal samples used in the experiment.

processing. According to the recommendation of the International Society of Rock Mechanics and Rock Engineering and the requirements of this true tri-axial impact experiment, each sample was processed into a 47 mm cube with height:diameter ratio of 1:1. Considering the structure of the coal, all samples were cut along the vertical bedding of a coal sample.

Each sample was polished to ensure that the parallelism at both ends of the sample was less than 0.02 cm, and the maximum deviation angle at both ends of the center line of a sample face was less than 0.25°. At the same time, before the experiment, in order to eliminate the influence of the end friction in the experiment as much as possible, the surface of each coal sample was coated evenly with lubricant. Through strict selection, processing and precise cutting of the coal samples, the experimental error was reduced as much as possible. Through the wave velocity test on a sample, the longitudinal wave velocity is:

$$v_p = \frac{L}{t - t_0} \quad (1)$$

where L is the distance of the longitudinal wave through a coal sample; t_0 and t are the excitation time and reception time of the longitudinal wave signal, respectively. For the processing requirements of coal sample stratification in this study, coal samples with close wave speed size and similar quality were selected for experimental testing.

Measurement Process

The experimental setup (Fig. 1) can effectively provide a source of dynamic loading for coal samples under different stress medium conditions and test the axial strain of coal samples, and many researchers have conducted similar experiments and analyzed the axial deformation characteristics of coal samples. There have been limited studies on stress waves and deformation properties of coal samples in both vertical and horizontal directions. Here, we developed a technique to analyze the tri-axial stress waveforms of coal samples.

As shown in Figure 3(1), strain gauges were used to test the horizontal (3#), axial (1#) and vertical (2#) stress wave signals of a square coal sample by attaching strain gauges to the axial, vertical and horizontal squares of the sample, respectively. After placing the sample with the affixed strain gauges into the experimental chamber, the leads of the strain gauges were sequentially connected to the Wheatstone bridge box (Fig. 3(2)). By switching on the hyperdynamic strain gauge (Fig. 3(3)), the three-way stress waveforms of the coal samples in the dynamic loading experiment can be acquired. Figure 3(4) shows the interface of stress waveform signal

acquisition for the coal sample. In this case, the static axial, vertical as well as horizontal pre-stresses of the sample were set in turn to 3, 2, 1 MPa. Varying dynamic impact speeds were achieved by positioning the bullet launcher at different locations, causing the bullet to travel through the infrared velocimeter at distances of L and 2.5 cm. Different impact speeds of the dynamic impacts were obtained by capturing the time of passing through the velocimeter as t . The dynamic impact velocity (v) was obtained by capturing the time of passing through the velocimeter as t , thus:

$$v = \frac{L}{t} = \frac{2.5 \times 10^{-2}}{t} (m/s) \quad (2)$$

For vibration loads on the coal samples in real working conditions, the impact velocities of the coal samples were set in turn to four impact velocities of 1.06, 1.17, 2.08 and 3.01 m/s.

Measurement Principle

Stress Test

As shown in Figure 4, the stress wave passes through the incident bar, the coal sample and the transmitted bar in turn, forming incident, reflected and transmitted waves. Figure 5a shows a typical stress wave schematic of the coal sample after being subjected to dynamic loading. The incident, transmitted and 1# waveforms were all negative, which is consistent with the direction of axial stress wave action. The reflected wave, 2# and 3# were all positive, showing a tension wave. The waveforms from the hop-bar and the anisotropy of the sample were significantly different. According to the force analysis of a sample, at the initial moment (0 ms as starting point), the stress wave first passed through the incident rod to form an incident wave, and then transmitted to the sample after about 0.4 ms, and all aspects of the coal body generated input waves. However, the waveform continued to enter the transmission rod with the direction of the σ_d , and the reflected and transmitted waves were generated at about 0.8 ms. At this stage, the anisotropic waveforms of coal samples all entered the decay stage.

According to the force schematic of a coal sample (Fig. 4), the forces F_1 , F_2 on the axial two end faces of the sample are (Gu et al., 2023b; Li et al., 2023b).

Deformation Characteristics and Mechanical Constitutive Model

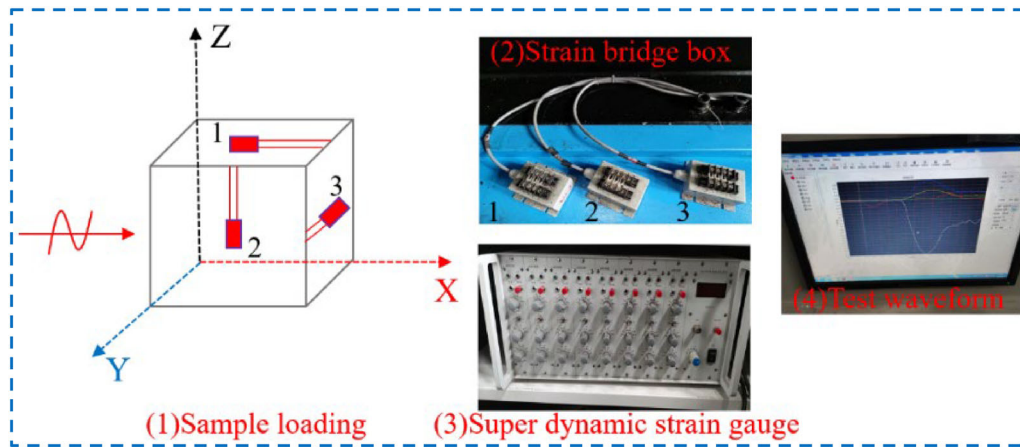


Figure 3. Triaxial stress wave test of coal.

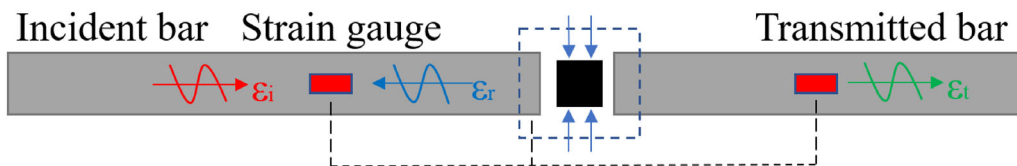


Figure 4. Effect of stress wave on coal sample.

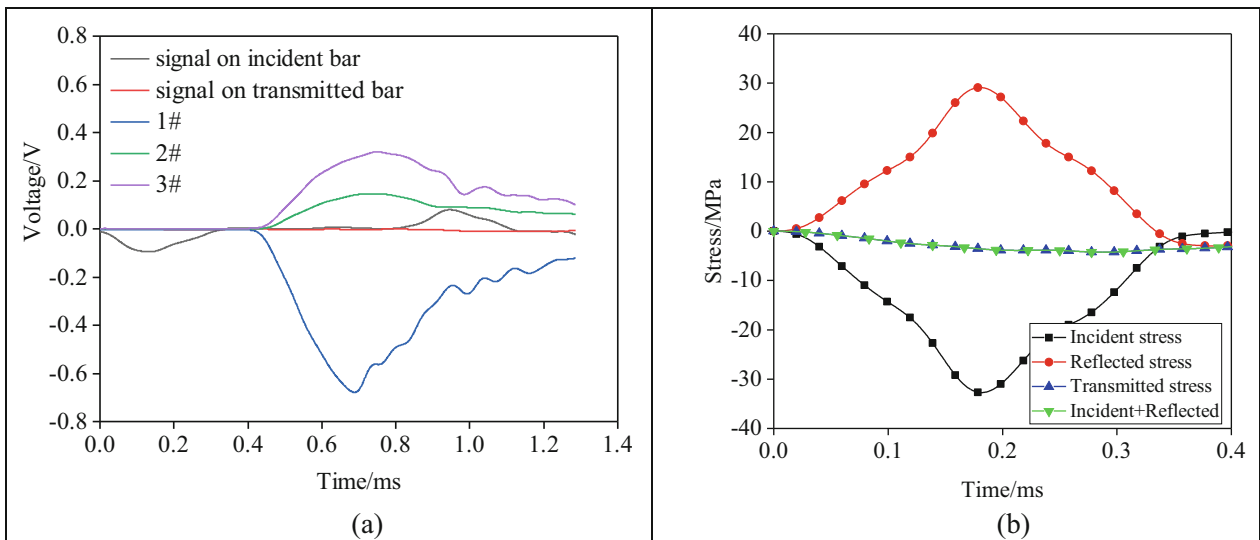


Figure 5. (a) Typical stress wave signal. (b) Stress balance verification.

$$F_1 = AE(\varepsilon_i + \varepsilon_r) + A_0\sigma_1 \quad (3)$$

$$F_2 = AE\varepsilon_t + A_0\sigma_1 \quad (4)$$

where A and E are the cross-sectional area and modulus of elasticity (210 GPa) of the compression rod, respectively; and A_0 and σ_1 are the cross-sectional area and axial pre-stress (3 MPa) of the coal sample, respectively.

From Figure 5b, assuming that the forces are balanced at both ends of a sample (Li et al., 2023c), the total force σ_t on the sample can be calculated as (Tan et al., 2023):

$$\begin{aligned} \sigma_t &= \sigma(t) + \sigma_1 = \frac{P_1 + P_2}{2A_0} \\ &= \frac{A}{2A_0} E[\varepsilon_i(t) + \varepsilon_r(t) + \varepsilon_t(t)] + \frac{2A_0}{2A_0} \sigma_1 \end{aligned} \quad (5)$$

Therefore, the dynamic stress in the sample should be:

$$\sigma(t) = \sigma_t - \sigma_1 = \frac{A}{2A_0} E[\varepsilon_i(t) + \varepsilon_r(t) + \varepsilon_t(t)] \quad (6)$$

where $\varepsilon_i(t)$, $\varepsilon_r(t)$ and $\varepsilon_t(t)$ are the incident, reflected and transmitted strains, respectively, of the sample at time t . Based on the stress wave curve of the coal sample in Figure 5a, the system device module can effectively calculate and obtain the axial dynamic stress of the coal sample. Part of the dynamic stress test results is shown in Figure 6.

Figure 6a depicts the dynamic stress variation curve of the coal samples, showing a gradual increase in peak stresses with rise in σ_d over time. The coal samples subjected to pre-stresses of 3, 0, 0 MPa were fragmented slowly, whereas those under pre-stresses of 3, 2, 1 MPa remained largely undamaged. Between 0 and 0.1 ms, the stress curve maintained a consistent upward trend. As time progressed, the stress curve quickly rose to its maximum point, indicating the duration of stress increase. Figure 6b indicates that a coal sample exhibits greater mechanical strength at 3, 2, 1 MPa than at 3, 0, 0 MPa. The coal samples exhibited greater mechanical strength when subjected to a 3 m/s load compared to a 2 m/s load. The coal samples reached peak stress faster under a 3 m/s σ_d at 3, 0, 0 MPa compared to 2 m/s, but took longer to reach peak stress under a 3 m/s σ_d at 3, 2, 1 MPa compared to 2 m/s. The results show that the internal fractures of the coal samples were more likely to expand and accelerate the damage under the condition of lack of

constraints, and the confining pressure made the coal samples free from damage. Figure 6d shows that with increase in deployment load, the stress rise rate of the coal samples increased significantly, and the stress rise rate was faster under uniaxial 3, 0, 0 MPa.

Stress Wave Testing

Under dynamic loading, the strain gauges connected to a coal sample will stretch and compress in response to the strain of the material being tested, causing a corresponding alteration in electrical resistance. The relationship between the change in resistance and the strain ε can be expressed as:

$$\frac{\Delta R}{R} = K \cdot \varepsilon \quad (7)$$

where R is the original resistance of the strain gauge, ΔR is the change in resistance caused by elongation or compression and K is a constant of proportionality (the strain gauge constant, which took a value of about 2).

Because strain change is fairly small, the resulting change in resistance is also extremely small. Whereas Wheatstone bridges are suitable for detecting small changes in resistance, the change in resistance of a strain gauge is measured using this circuit. Connecting R_I in the circuit with a strain gauge, when there is a change in strain, denoted as ΔR , and the input voltage before the strain test is E (Fig. 7), the formula for the output voltage e is:

$$e = \frac{1}{4} K \cdot \varepsilon \cdot E \quad (8)$$

So, when the output voltage e of the bridge is measured, the strain ε of a sample can be calculated as:

$$\varepsilon = \frac{4e}{k \cdot E} \quad (9)$$

By utilizing the experimental apparatus described above and understanding the experimental concept, the stress wave curve of the coal samples under triaxial conditions can be generated following a full impact test, allowing for the calculation of a coal sample's anisotropic strain. In contrast to previous studies by certain academics that concentrated on uniaxial stress-sweep and strain collection, this experimental test plan clearly captured two additional directional strain parameters, providing valu-

Deformation Characteristics and Mechanical Constitutive Model

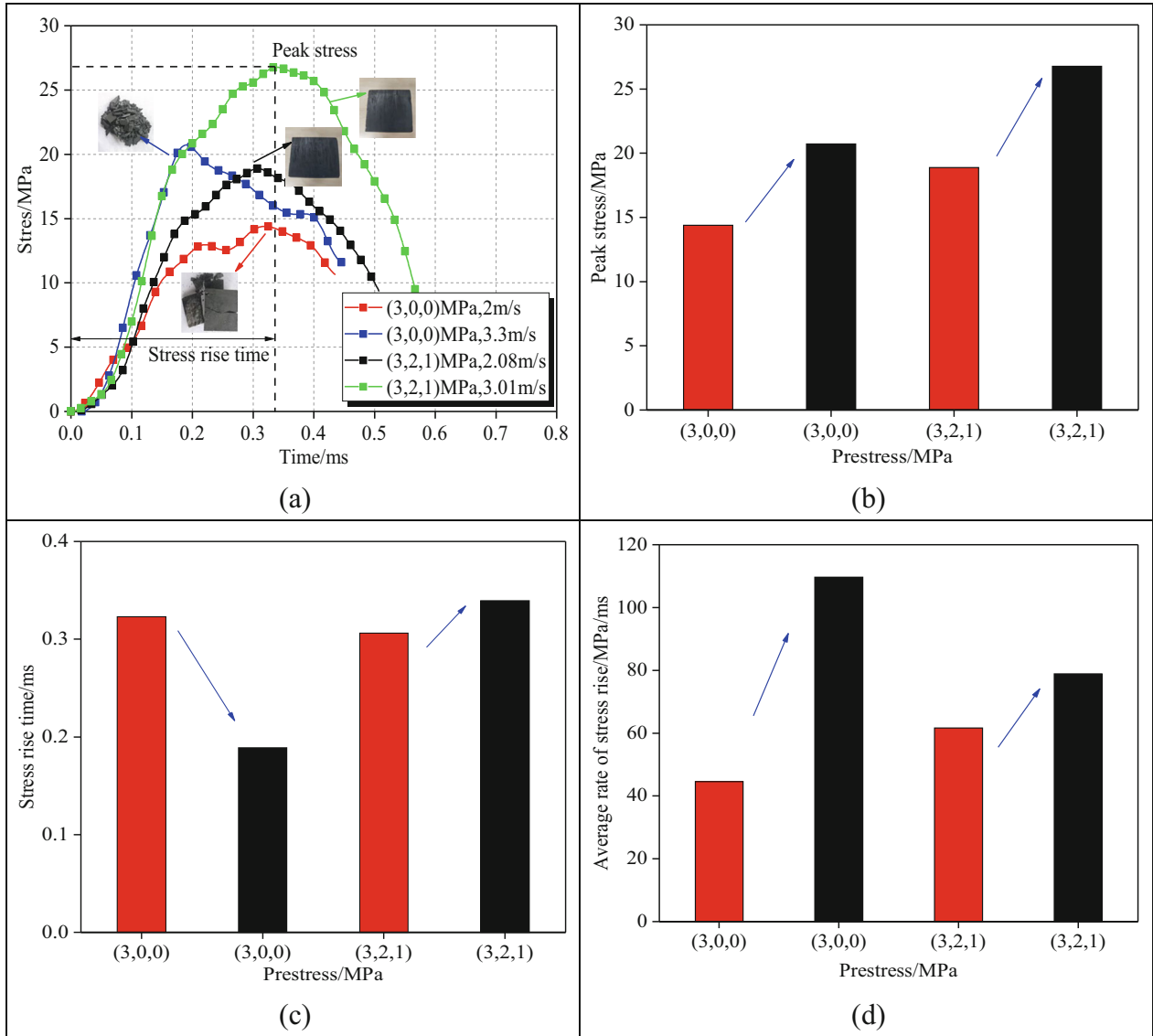


Figure 6. Kinetic parameter analysis of coal sample.

able guidance for analyzing stress-sweep and strain variations in coal samples.

EXPERIMENTAL RESULTS

Strain Evolution Pattern

As shown in Figure 8, the strain in the X, Z and Y directions of the coal samples changed slowly at the beginning. With increase in time, the strain change trend of the coal samples accelerated grad-

ually, in which the strain in X direction increased the fastest. This is due to the fact that the direction of the σ_d force is along the X direction. When the deformation of the sample reached a certain value and then decreased gradually, the strain of sample from 0 to the maximum value of the whole process lasted about 0.3 ms. The test strain was positive in the X direction, while it was negative in the Z and Y directions for the coal sample. The lateral force on the coal sample under σ_d caused expansion deformation, while compression deformation occurred in the axial direction.

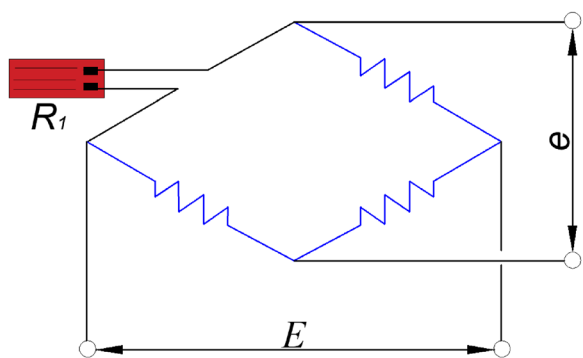


Figure 7. Principles of strain calculation.

Maximum Strain Law

By defining the strain maximum in Figure 8 as the maximum strain, the maximum strain deformation pattern of the coal samples under different impact velocities is shown in Figure 9. With increase in v , the maximum strain in X, Z and Y directions all increase gradually and linearly. The deformation pattern of coal samples in the X direction was the most significant, the strain in the X direction of the coal samples increased from 0.00323 to 0.00656 as the v increased from 1.06 to 3.01 m/s; the strain in the Z direction of the coal samples increased from

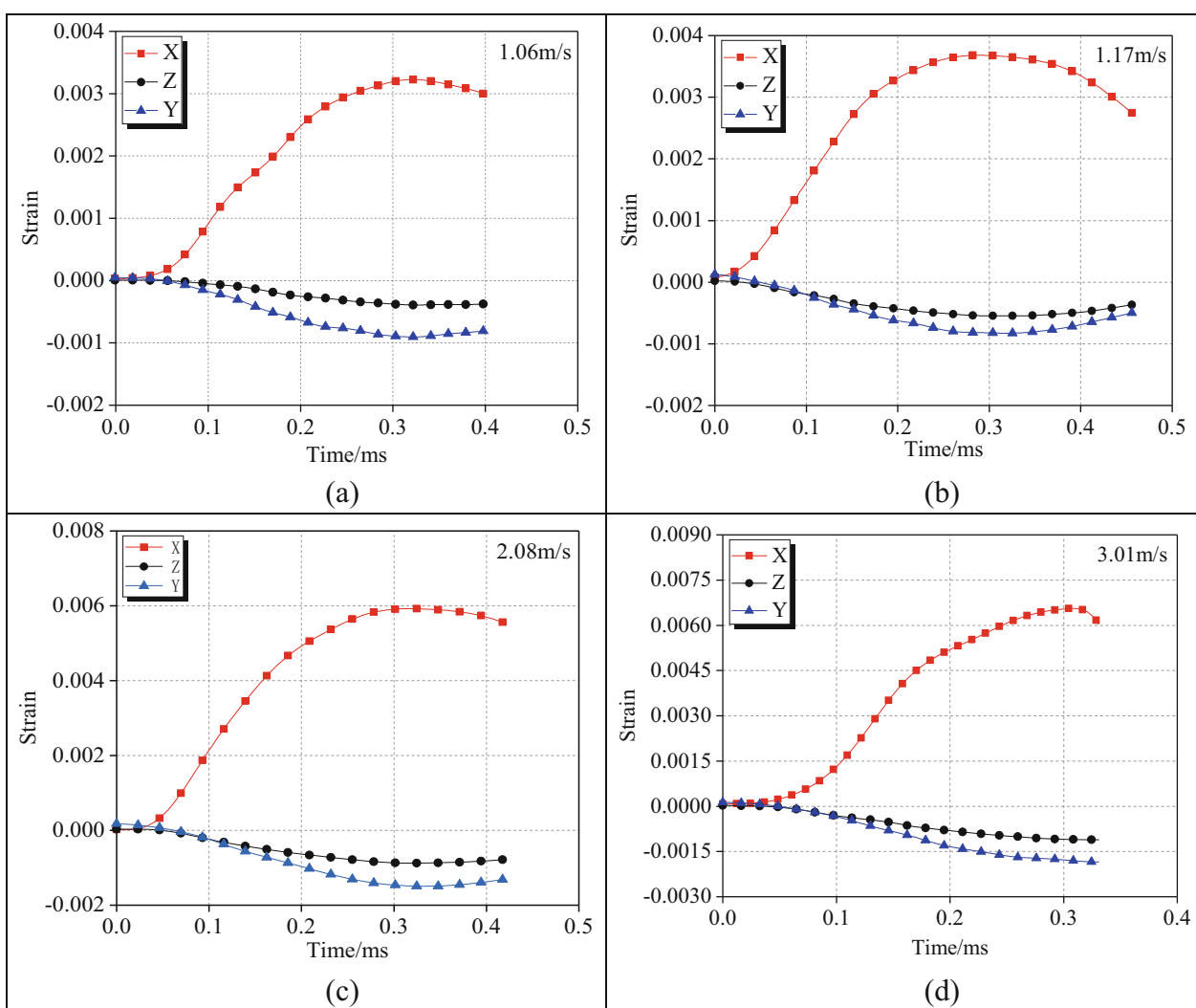


Figure 8. Triaxial strain characteristics of coal samples.

Deformation Characteristics and Mechanical Constitutive Model

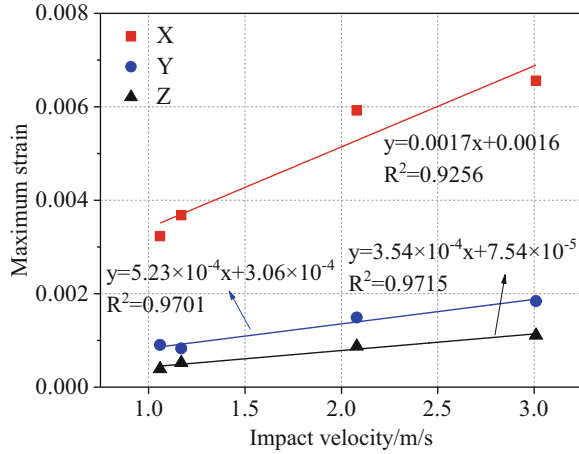


Figure 9. Maximum strain law of coal.

0.0003915 to 0.00111, and that in the Y direction of the coal samples increased from 0.0009045 to 0.00184.

By taking the ratio of the maximum strain in the Y and Z directions to the maximum strain in the X direction, the following are defined:

$$\eta_Z = \frac{|\varepsilon_Z^m|}{\varepsilon_X^m} \quad (10)$$

$$\eta_Y = \frac{|\varepsilon_Y^m|}{\varepsilon_X^m} \quad (11)$$

The study revealed that the η_Z values ranged 0.12–0.17 while the η_Y values ranged 0.22–0.28 for impact velocities of 1.06–3.01 m/s. The coal samples deformed primarily along the X-axis when subjected to dynamic loading in the axial direction. Expansion deformation in the vertical and horizontal directions was found to be less significant than axial deformation.

Waveform Characteristics

By testing the axial stress wave on the coal samples, the waveforms were obtained (Fig. 10a). When the σ_d was applied to the coal samples, the stress wave amplitude decreased rapidly, showing a compression wave. When the stress wave reached the maximum magnitude, it rose sharply, and then the whole exhibited a recurring trend of rising and falling. However, the whole showed a trend of stress wave attenuation. Due to the existence of axial pre-

stressing, the sample was not completely compression wave, the decay process was also accompanied by the appearance of tensile wave, but the maximum magnitude of the tensile wave was smaller than the amplitude of the compression wave. When the v was 1.06 m/s, after the stress wave action time was 15 ms, the amplitude of the stress wave was mainly in the positive range and was dominated by tensile wave. When the v was 1.17 m/s, the stress wave finally decayed to the positive value interval as well. This is due to the low v acting on the coal samples, and the coal samples themselves carried a static pre-stress of 3 MPa, which contributed to the limited deformation of the coal samples. When the v reached 2.08 m/s and 3.01 m/s, the stress wave tended to flatten out and with increase in time tended to 0. Obviously, due to the increase of the σ_d applied to the coal sample, the σ_d played a more significant role in the change of the stress wave compared with the limited deformation of the coal sample by the axial pressure.

Figure 10b and c shows the vertical and horizontal stress waveforms of the coal samples, respectively. Compared with Figure 10a, the stress waves both showed a gradual decay pattern with increase in time. However, compared with the axial stress waveform, which was dominated by compression wave, the vertical and horizontal stress waveforms were dominated by tensile wave. The coal samples were originally under static pre-stress of 3, 2, 1 MPa, and when subjected to the dynamic loaded stress wave, the stress wave showed a tendency of rapid increase and subsequent decay. The change of the waveform of the stress wave was more significant in the range of 0–10 ms, followed by a slower change in the range of 10–40 ms.

Spectral Analysis

The stress waveform in Figure 10 demonstrates that the stress wave was induced on all sides of the sample when it was subjected to the incident bar, with the most noticeable change occurring in the axial direction. According to research of related scholars, the total wavelength L of stress wave propagation from the incident bar to the sample and then to the transmission bar should be (Han et al., 2022):

$$L = CT \quad (12)$$

The propagation velocity of the stress wave in this study was 5100 m/s, and the action time of a

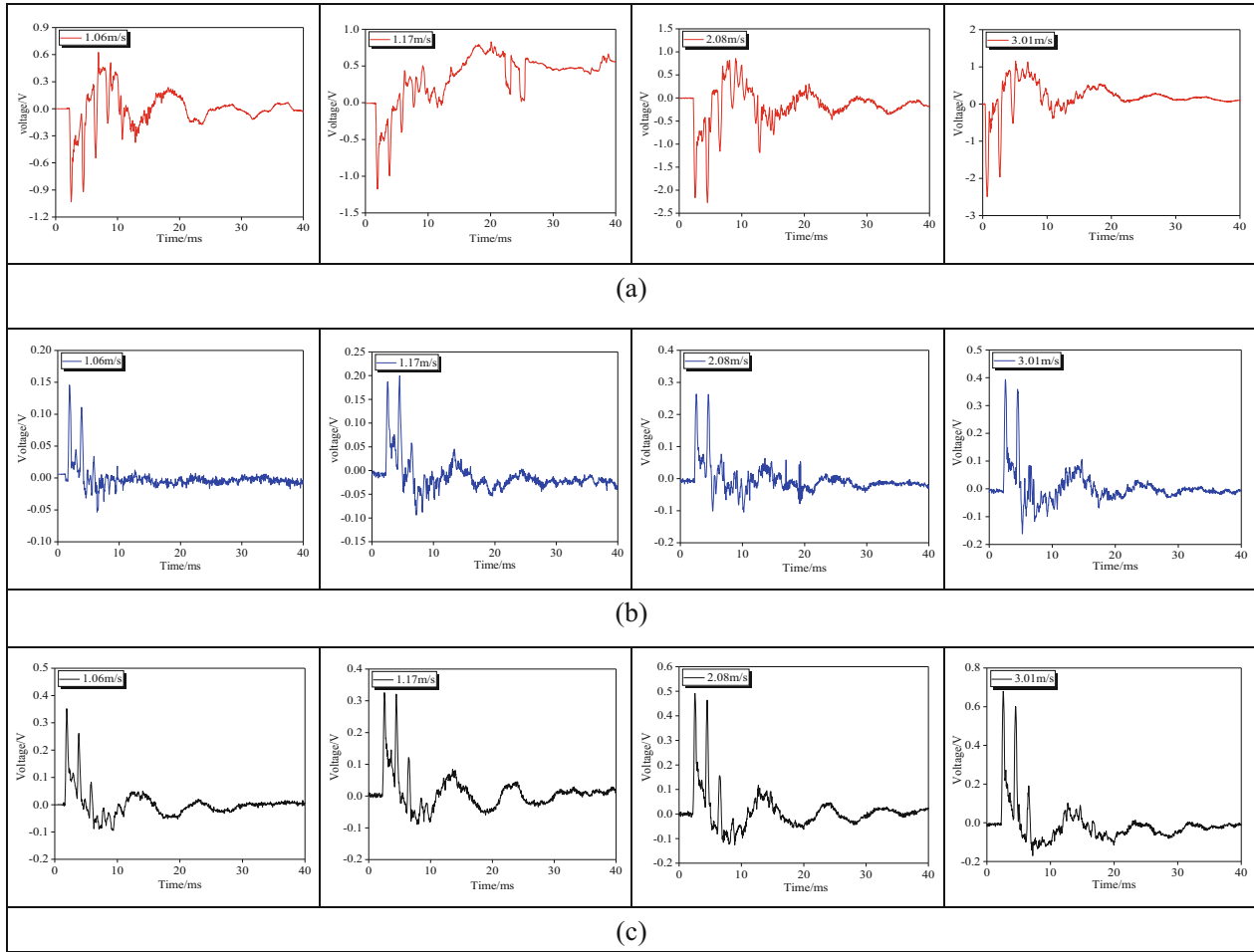


Figure 10. Curve of three-way stress waveform: (a) axial stress waveform; (b) vertical stress waveform; (c) horizontal stress waveform.

single stress wave was about 0.3–0.4 ms, then L was calculated to be about 2 m. And the size of the sample was about 47 mm, indicating that the strain signal captured on the sample was a superposition of multiple reflections and transmissions. Therefore, Fourier transform was considered to analyze the spectrum of waveform transformation (Wang et al., 2023):

$$F(w) = \int_{-\infty}^{\infty} f(t)e^{-j\omega t} dt \quad (13)$$

where $f(t)$ is the continuous time signal function, and $e^{-j\omega t}$ is the basis function of the Fourier transform.

As shown in Figure 11a, the main frequency of the stress wave was distributed mainly within 0–10 kHz, and the amplitude signal varied more drastically. The main peak was located within 0–

10 kHz, and the main peak showed a decreasing trend. The overall pattern of the stress wave spectrum under different impact speeds was relatively similar. As the σ_d increased, the spectrum's amplitude rose gradually. Comparing Figure 11b and c, the spectra of vertical and horizontal stress waves were similar to those of axial stress waves, and the main frequency was distributed mainly within 0–10 kHz, and the amplitude became larger with increase in σ_d . However, the maximum amplitude of the spectrum was smaller than that of the axial stress wave. It shows that, when the stress wave acts on a coal body, all of its directions are affected by the stress wave at a similar time, but the axial direction belongs to the direction of the σ_d , and the sample suffers from the most obvious dynamic impact damage of the stress wave.

Deformation Characteristics and Mechanical Constitutive Model

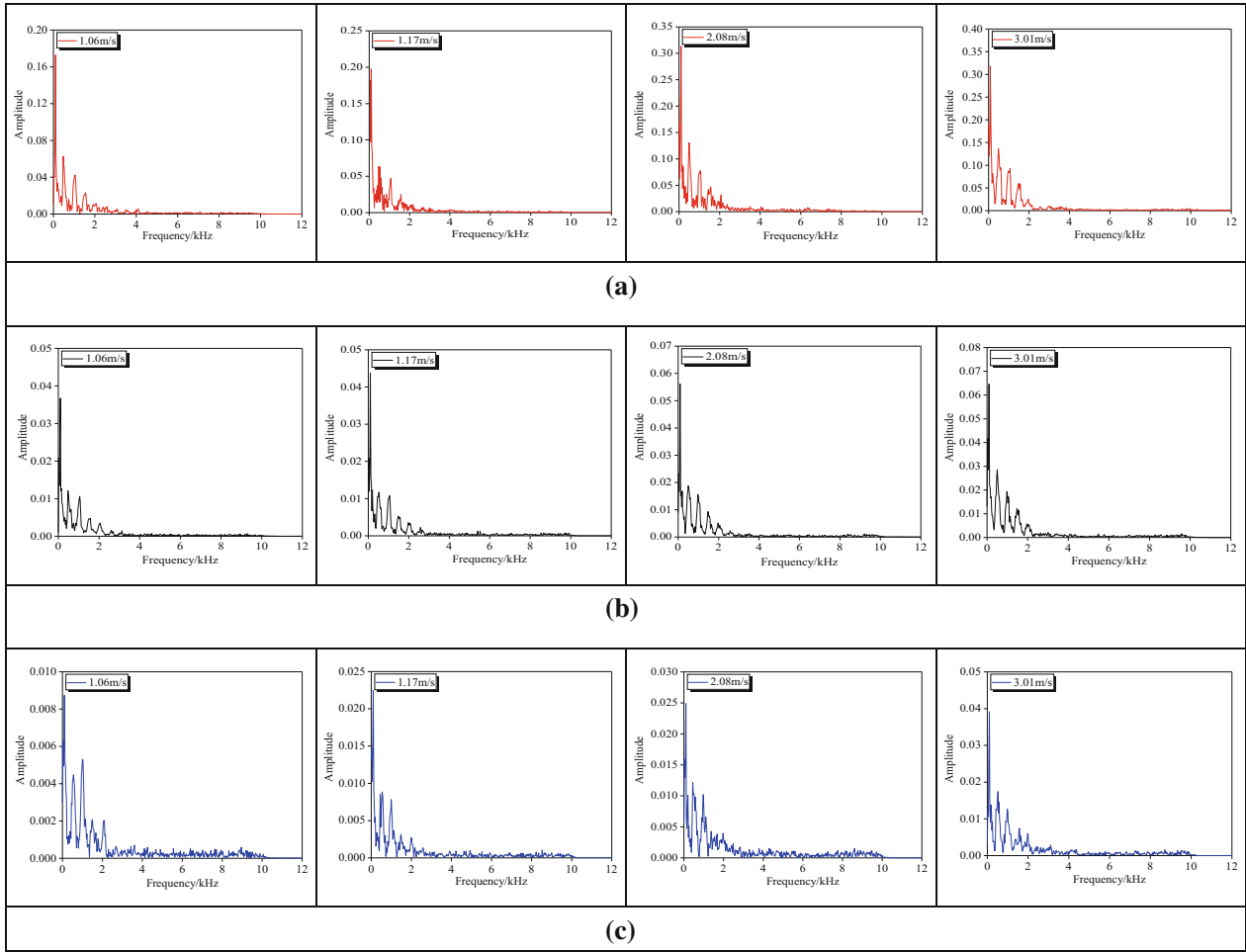


Figure 11. Stress wave spectral analysis: (a) axial direction; (b) upright; (c) level.

DISCUSSION

Stress Wave Characteristics

The stress waveforms shown in Figure 10 reveal that the axial, vertical and horizontal stress waves in the coal samples were decaying gradually after the σ_d was applied to the samples. Referring to a previous study on the decay process of the stress wave of coal samples (Wang et al., 2022a, 2022b), as shown in Figure 12, the incident and transmitted waves of the stress wave of coal samples captured by the strain gauges affixed to the incident and transmitted rods showed a gradual decay process with increase in time. Obviously, the attenuation signals on the incident and transmitted rods were to some extent similar to the attenuation law of the axial

stress waveforms tested on the coal sample surface. Therefore, to prevent dynamic disaster produced by stress wave on coal rock, stress should be prevented from the source as much as possible and reduce the stress fluctuation loading effect in time.

Referring to studies of some scholars, as shown in Figure 13, it was concluded that the spectral activity of the stress wave of the rock samples penetrated with intercalation was within 0–30 kHz, and the distribution of the main frequency spectrum of the stress wave of the rock samples was within a certain range (Han et al., 2022). Jin et al. (2020) also worked out that the main frequency of the stress wave of the rock is within 0–3 kHz. Based on Figure 11, it is concluded that the active frequency of the stress wave of the coal body was distributed mainly within 0–10 kHz, and the maximum magni-

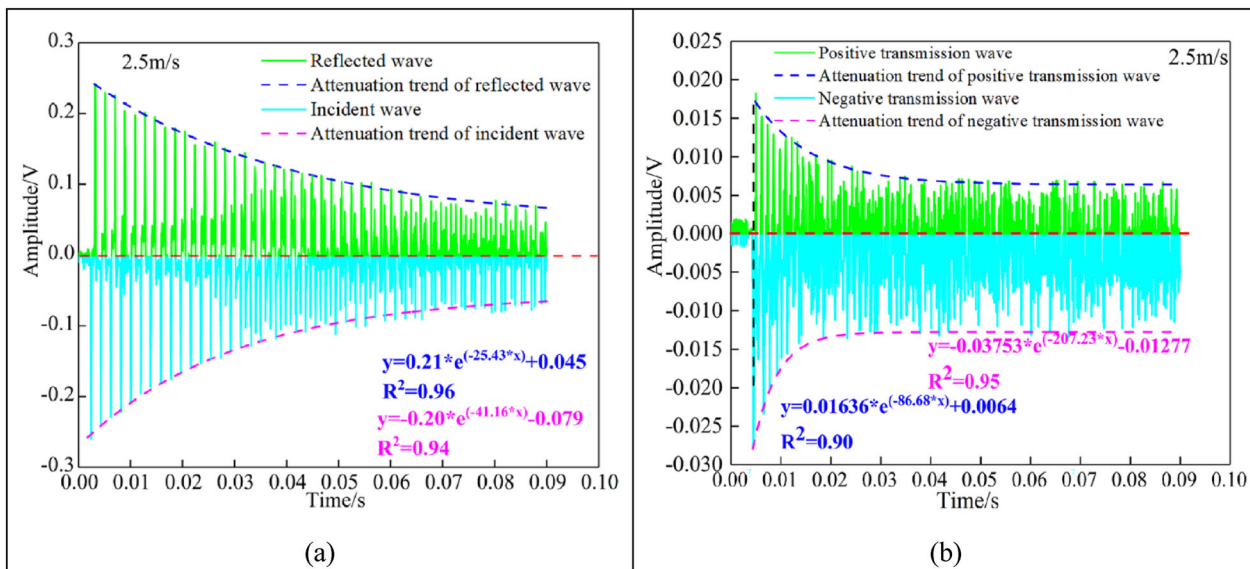


Figure 12. Stress wave signal attenuation (Li et al., 2023b).

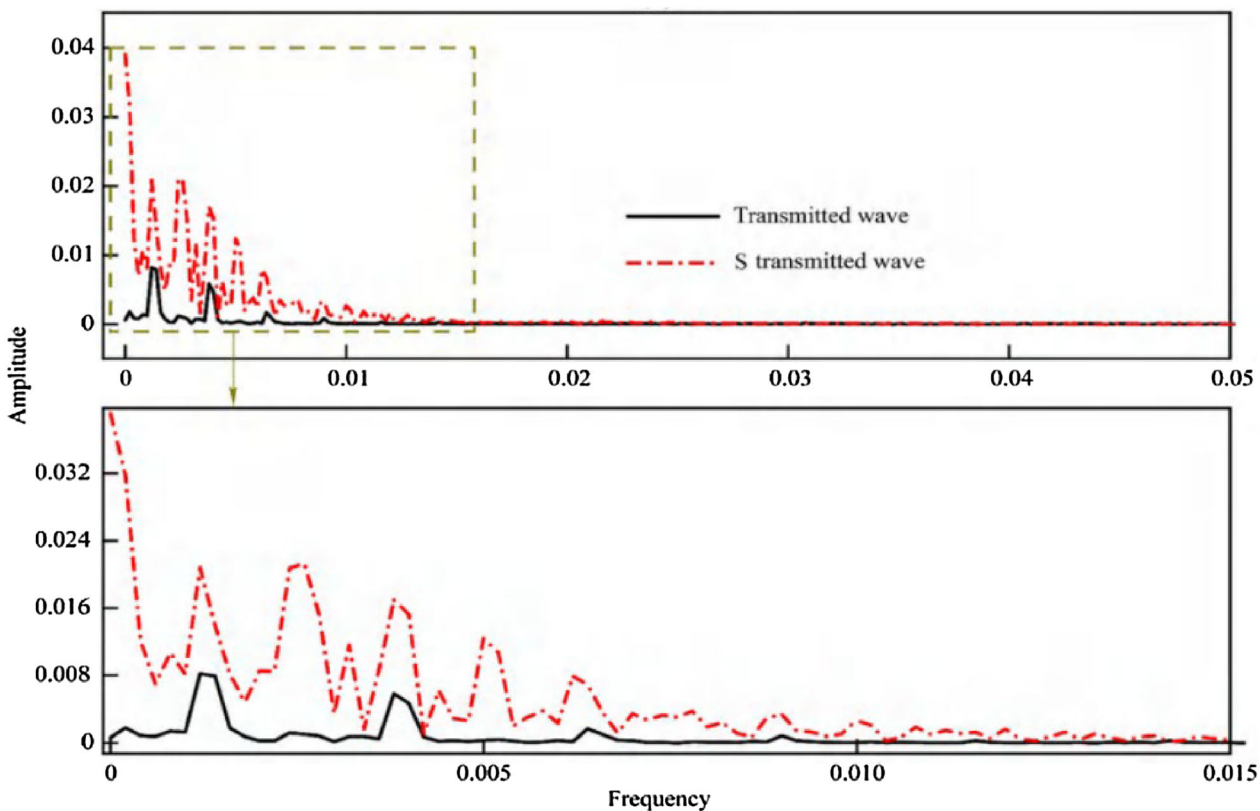


Figure 13. Spectral analysis of rock (Han et al., 2022).

Deformation Characteristics and Mechanical Constitutive Model

tude increases with increase in v (Jin et al., 2020). According to our findings and those of previous scholars, the spectrum of coal and rock and other materials are distributed in the low-frequency range, and the larger the σ_d stress wave is, the larger the maximum magnitude of the spectrum is.

Meanwhile, compared with previous researches, most of them rely on strain gauges on the incident and transmission rods to obtain the stress waveforms, and mainly carry out one-dimensional tests on coal and rock bodies. However, the present test methodology can effectively simulate stress wave changes of coal rock body under three-dimensional (3D) unequal stresses after being subjected to σ_d , which make the study of stress wave characteristics of coal rock body closer to the field engineering reality. Various alterations in triaxial stress and σ_d can greatly impact the physical characteristics of coal samples, while the testing equipment is capable of accurately detecting stress waves in coal rock.

Stress Wave Attenuation Analysis

Because the dynamic impact direction of the coal samples was consistent with the direction of σ_1 , the axial direction had the most significant stress wave and strain changes due to the combined dynamic and static load forces. Based on research of relevant literature (Li et al., 2023a; Shen et al., 2023), the incident (E_i), reflected (E_r) and transmitted (E_t) energy of a coal sample can be calculated, respectively, as:

$$E_i = AEC \int_0^t \varepsilon_i^2(t) dt \quad (14)$$

$$E_r = AEC \int_0^t \varepsilon_r^2(t) dt \quad (15)$$

$$E_t = AEC \int_0^t \varepsilon_t^2(t) dt \quad (16)$$

Based on the calculated E_i , E_r and E_t , the energy absorption (N) of a coal sample can be defined as (Han et al., 2020; Fan et al., 2021; Yan et al., 2021; Du et al., 2023):

$$N = \frac{E_i - E_r - E_t}{E_i} \times 100\% \quad (17)$$

As shown in Figure 14, the values of N increase linearly with increasing v . The coal sample initially

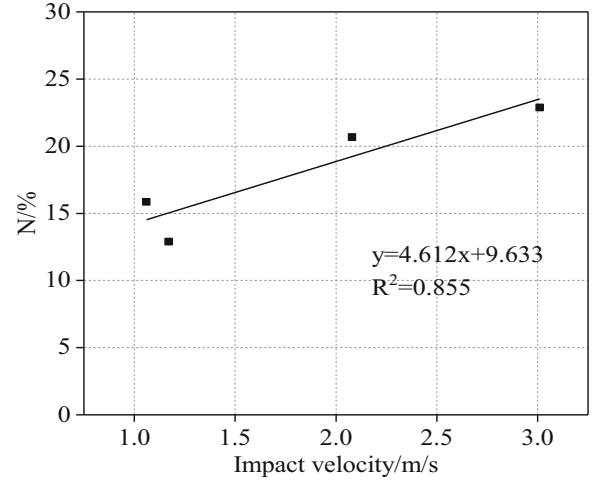


Figure 14. Energy absorption rate of coal samples.

had low deformation and intact morphology, and the required energy consumption was low. Raising the velocity at which the impact occurs raised the energy involved in the event, causing cracks in the sample to widen and worsen the damage to the coal sample. This ultimately resulted in the coal absorbing more energy when subjected to the stress wave. The gradual increase of stress wave is synchronous with the process of damage intensification of coal samples.

The propagation characteristics of ultrasonic waves in coal rock are closely related to its physical and mechanical properties. From the theory of elastic wave correlation, the theoretical formula for the longitudinal wave propagation velocity v_p in coal rock is (Zhou et al., 2023a, 2024):

$$v_p = \sqrt{\frac{3K(1-\mu)}{\rho(1+\mu)}} \quad (18)$$

where K is bulk modulus (Pa), ρ is density (kg/m^3) and μ is Poisson's ratio.

The macroscopic damage characteristics of the coal samples under different impact velocities were investigated by analyzing the change rule of wave velocity. Based on the measurements of the v_p and v of the coal samples before and after impact, the damage variable (D) of a coal sample subjected to stress waves was calculated as (Gong et al., 2023).

$$D = \left(1 - \frac{v^2}{v_p^2}\right) \times 100\% \quad (19)$$

As shown in Figure 15, when the v was about 1 m/s, the D was only about 5%, and there was almost no damage to the coal samples. When the v was about 3 m/s, the damage variable reached about 18.5%, and the damage to the coal samples increased. When the v increases from 1 to 3 m/s, the overall damage variable showed a linear increase. Meanwhile, in combination with Figure 14, the more damage detected during ultrasonic analysis, the higher the energy absorption rate of coal samples. Moreover, it indicates a relationship between the stress wave and spectral amplitude of coal samples with both energy consumption and damage.

In engineering practice, most working conditions can monitor or control the size of the v . The degree and extent of macro damage to the coal body can be determined by analyzing the v and verifying the feedback with ultrasonic testing. This information can be used as a reference for engineering and construction design.

REFERENCE TO STRESS WAVE EVOLUTION FOR ENGINEERING APPLICATIONS

Stress changes in a quarry are often a precursor to the occurrence of dynamic disasters, which have different initiating effects on the coal rock impact at the working face. In the process of stress wave action, the stress balance of the surrounding rock in the coal rock roadway is destroyed. The σ_d and static load act together on coal rock, and the larger the σ_d

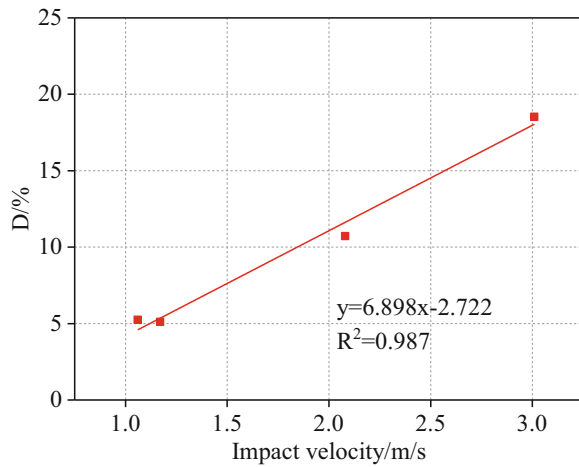


Figure 15. Coal damage analysis based on the wave velocity.

is, the three-directional stress waves of the coal body have significant changes, among which the changes are most obvious along the direction of stress wave transmission (Fig. 16). The static loads σ_2 and σ_3 are provided to limit the deformation of a coal body (Zhou et al., 2023b), and the deformation of a stressed surface under σ_2 pre-stress condition is smaller. So, when σ_3 is increased to σ_2 so that the forces in both directions are equal, the deformation of a coal sample will be reduced. Or, reducing σ_d , that is, reducing the generation of σ_d stress wave, reduces the deformation produced by a coal body. Therefore, in a comprehensive analysis, the stress wave (SW) influencing factors of a coal rock body can be expressed as:

$$SW \doteq \begin{cases} \sigma_d \\ \sigma_s \\ \sigma_d + \sigma_s \end{cases} \quad (20)$$

When the dynamic stress wave σ_d or static pre-stressing force σ_s is large enough, the coal body is deformed and damaged. When static pre-stress is not enough to damage a coal body, the provision of a certain size of dynamic pre-stress ($\sigma_d + \sigma_s$) damages a coal body. Based on the stress wave study of a coal body under three-way pre-stress in this study, it is concluded that high static load, high σ_d stress wave and the coupling effect of static load and stress wave can damage a coal rock body. In the future, the device used here can be utilized to analyze the stress wave of various types of coal and rock materials, uncovering the failure mechanism of critical static and dynamic loads in complex stress environments.

MECHANICAL CONSTITUTIVE MODEL

Model Construction

The coal rock is believed to be made up of numerous tiny particles that are large in size spatially, allowing for many micro-defects, yet small enough in the mechanical sense to be considered a particle. Given that a cell's power adheres to the Weibull distribution, the probability density function $\varphi(F)$ is represented as (Zang et al., 2024a):

$$\varphi(F) = \frac{m}{F_0} \left(\frac{F}{F_0} \right)^{m-1} \exp \left[- \left(\frac{F}{F_0} \right)^m \right] \quad (21)$$

where F is a random variable of the Weibull function, and m and F_0 are the distribution parameters.

Deformation Characteristics and Mechanical Constitutive Model

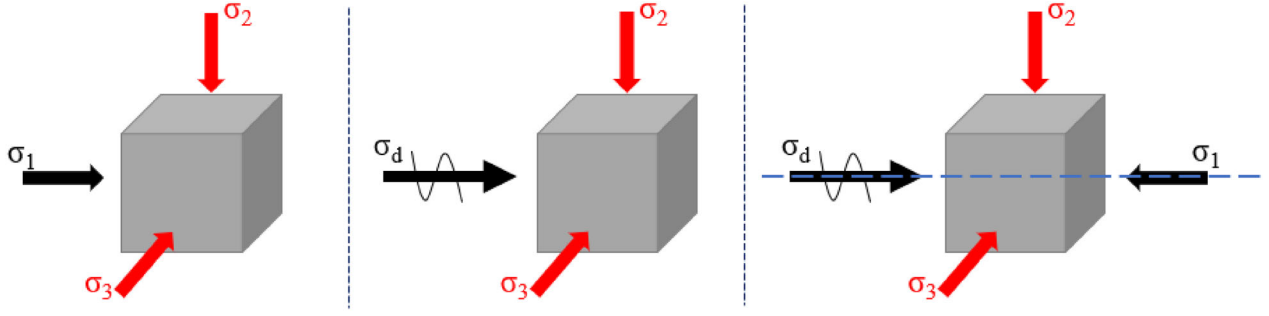


Figure 16. Anisotropic stress analysis of coal.

Then, the statistical damage variable D can be defined as (Zang et al., 2024b):

$$D = \frac{N_d}{N} \quad (22)$$

where N_d is the number of elements and N is the total number of elements. According to Eqs. (21) and (22), the relationship between D and F can be obtained as (Kong et al., 2021):

$$D = 1 - \exp\left[-\left(\frac{F}{F_0}\right)^m\right] \quad (23)$$

Due to the three-way pre-stresses σ_1 , σ_2 and σ_3 of a coal body in this study, the D - P criterion can be considered under the constraint of multidimensional pre-stressed stress, and the strength criterion can be expressed as:

$$F = f(\sigma) = \delta_0 I_1 + \sqrt{J_2} \quad (24)$$

where the relevant parameters can be expressed as (Xie et al., 2022a, 2022b):

$$\begin{cases} \delta_0 = \frac{\sin\theta}{\sqrt{3(3+\sin^2\theta)}} \\ I_1 = \sigma_1^* + \sigma_2^* + \sigma_3^* \\ J_2 = \frac{1}{6} [(\sigma_1^* - \sigma_2^*)^2 + (\sigma_2^* - \sigma_3^*)^2 + (\sigma_1^* - \sigma_3^*)^2] \end{cases} \quad (25)$$

where θ is the internal friction angle of a coal sample (30°), and σ_i^* corresponds to the nominal stress σ_i . The effective σ_i^* of coal under three-way pre-stress can be expressed as:

$$\sigma_i^* = \frac{\sigma_i}{1-D} \quad (26)$$

According to Hooke's law, by combining the force of a coal sample with the static pre-stress σ_1

and σ_d along the impact direction, and the lateral binding force σ_2 and σ_3 , the axial strain ε of a coal sample can be expressed as:

$$\varepsilon = \frac{1}{E} \left(\frac{\sigma_d + \sigma_1 - \nu_2 \sigma_2 - \nu_3 \sigma_3}{1-D} \right) \quad (27)$$

Then, the mechanical model of a coal sample under true triaxial conditions can be determined as:

$$\sigma_d = E\varepsilon(1-D) - \sigma_1 + \nu_2 \sigma_2 + \nu_3 \sigma_3 \quad (28)$$

Combined with Eqs. (23) and (27), the mechanical model can be expressed as:

$$\sigma_d = E\varepsilon \exp\left[-\left(\frac{F}{F_0}\right)^m\right] - \sigma_1 + \nu_2 \sigma_2 + \nu_3 \sigma_3 \quad (29)$$

Model Verification

According to Eq. (29), the values of m and F_0 need to be solved. Therefore, the derivation of formula (29) is obtained by combining experimental data and extreme value method (Kong et al., 2021):

$$\begin{aligned} \frac{\partial \sigma_i}{\partial \varepsilon_i} \Big|_{(\sigma_p, \varepsilon_p)} &= E \exp\left[-\left(\frac{F}{F_0}\right)^m\right] + E \varepsilon \exp\left[-\left(\frac{F}{F_0}\right)^m\right] \\ &\quad \cdot (-m) \cdot \left(\frac{F}{F_0}\right)^{m-1} \cdot \frac{1}{F_0} \frac{\partial F}{\partial \varepsilon} \\ &= 0 \end{aligned} \quad (30)$$

Equation (30) can be rewritten as:

$$m \cdot \left(\frac{F}{F_0}\right)^m \frac{\varepsilon}{F} \frac{\partial F}{\partial \varepsilon_i} \Big|_{(\sigma_p, \varepsilon_p)} = 1 \quad (31)$$

The, from Eq. (24), (25), (29), (30) and (31), it can be obtained that:

Table 1. Model correlation parameter

No.	v /m/s	σ_1	σ_2	σ_3	ε_m	E /GPa	ν_2	ν_3
1	2.08	3	2	1	0.0057	18.822	0.147	0.251
2	3.01	3	2	1	0.00816	28.058	0.169	0.28

$$m = 1 \quad (32)$$

According to Eqs. (29) and (31), the constitutive model can be further improved as:

$$\sigma_d = E\varepsilon \exp\left[-\left(\frac{F}{F_0}\right)\right] - \sigma_1 + \nu_2\sigma_2 + \nu_3\sigma_3 \quad (33)$$

According to the constitutive model in Eq. (33), the peak stress σ_p and strain ε_p are obtained from experimental data, and ν_2 and ν_3 are approximated by reference Eqs. (10) and (11), respectively, and can also be considered as measured parameters. Figure 16 shows the curve obtained by the model and the curve measured by the experiment. The relevant parameters of the constitutive model are shown in Table 1.

The model reflects well the relationship between mechanical strength, σ_d and three-way pre-stress ($\sigma_1, \sigma_2, \sigma_3$) of coal. Moreover, the overall degree of fit of the theoretical curve to the experimental curve is well taut (Fig. 17). Of course, there is still some gap between the slope of the theoretical curve and the linear elastic stage of the coal mechanical curve. In the future, the model can be improved further from the perspective of the strain slope selection of the linear elastic stage or the strain rate of the coal. However, combined with the testing method, the mechanical constitutive model of true 3D coal is well analyzed. Compared with the empirical values of a large number of conventional ν , the measured values of lateral constraints of coal are reflected in this study, which are closer to the measured mechanical curves.

This paper focused on the study of the stress wave variation characteristics of coal samples under true triaxial conditions and will continue in the future to carry out cyclic impact and non-isocyclic impact tests (Liu et al., 2024; Zhang et al., 2024) with different impact velocities. Based on the single ν in this study, the stress wave variation of coal samples will be analyzed further. At the same time, only the waveform changes were obtained for the stress waves of coal samples. In the future work, we will try to use ultrasonic detector (Luo et al., 2022; Wang et al., 2024), optical fiber (Du et al., 2021), acous-

toelectric monitoring (Liu et al., 2023; Zhang et al., 2023), potential (Zang et al., 2024a, 2024b, 2024c) and computer tomography (Liu et al., 2019) to invert the damage conditions of coal samples, so as to form a comparative analysis with the stress wave changes of coal samples. It will be helpful to further study the stress wave characteristics of coal samples.

CONCLUSIONS

The dynamic mechanical properties of coal samples under three-way circumferential pressure were investigated experimentally using a three-way circumferential pressure dynamic impact loading experimental device, and the three-way stress wave and strain characteristics of coal samples under vibration loading were analyzed. The coal sample experienced lateral stress waves and stress waves in the impact direction, which exhibited tension and compression waveforms, respectively.

The strain of the coal samples under three directions of stress was greatly affected by the shock load, and the maximum strain increased linearly with increase in impact velocity. From 1 to 3 m/s, the maximum strain in the X direction (3 MPa pre-stress) increased from 0.00323 to 0.00656, and the maximum strain in the Y (2 MPa pre-stress) and Z (1 MPa pre-stress) directions increased from 0.000904 to 0.00184 and from 0.000391 to 0.00111, respectively. The strain of the coal sample in the axial impact direction with binding force of 3 MPa was the largest, while the strain of the coal sample in the lateral binding force of 2 MPa was smaller than that in the lateral binding force of 1 MPa. These show that the impact load causes the deformation of a coal sample, and the increase of binding force limits the deformation of a coal sample.

The three-way stress waves of coal sample deformation all showed first increase and then gradual decrease with increase in time, and the overall evolution of the stress waves was a gradual attenuation process. The dominant frequency of the stress wave was distributed in the range of 0–10 kHz, and the amplitude of the stress wave spectrum showed a positive correlation with change in impact velocity. The stress wave and spectrum amplitude of the coal sample along the axial impact direction (3 MPa pre-stressing) were the largest, and the stress wave and spectrum amplitude of the coal sample when the lateral binding force was 2 MPa were smaller than that when the lateral binding

Deformation Characteristics and Mechanical Constitutive Model

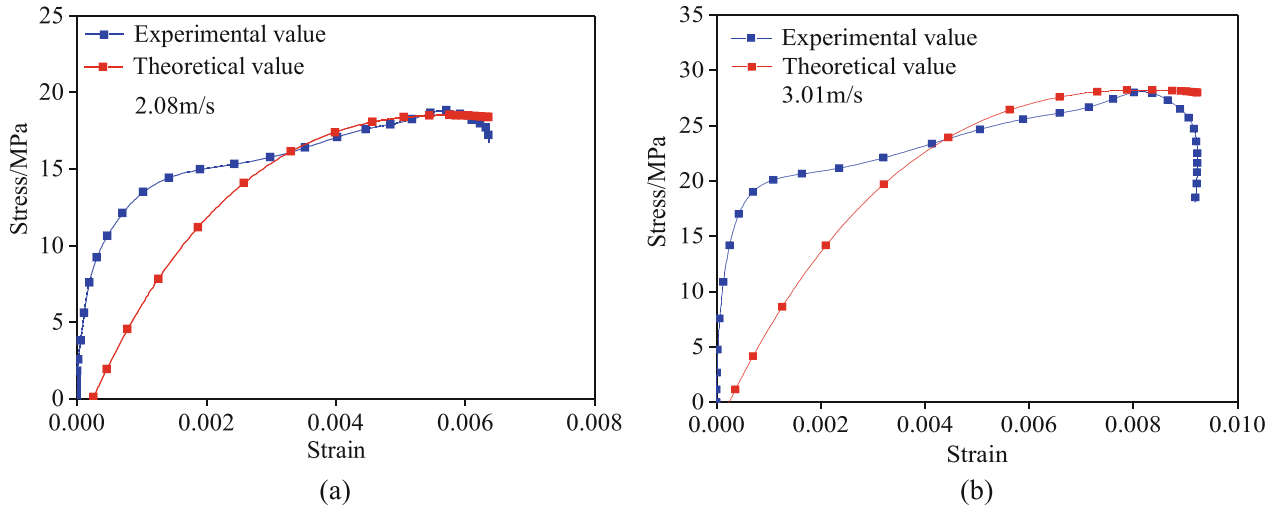


Figure 17. Curves obtained by constitutive model and measured curves.

force was 1 MPa. These show that the impact load promotes the stress wave transmission more than the lateral binding force.

The generation of stress waves in coal samples was correlated with both the static load as well as the dynamic load applied. It is shown that high static load, high dynamic load stress wave and coupling effect of static load and stress wave can damage the coal rock body. Due to the combined static and dynamic loads on the axial direction of the coal samples, the magnitude of the stress waves was much higher than that of the vertical and horizontal stress waves. Based on the energy absorption as well as the change of ultrasonic velocity, the damage N value of a coal body under 1 to 3 m/s dynamic load increases from 15.86% to 22.88% and from 5.24% to 18.52%, respectively. This shows that coal damage gradually increases with vibration load.

Combined with the force analysis of coal sample (i.e., σ_d , σ_1 , σ_2 , σ_3), a dynamic model of a coal sample under true triaxial condition is proposed: $\sigma_d = E\varepsilon \exp\left[-\left(\frac{F}{F_0}\right)\right] - \sigma_1 + \nu_2\sigma_2 + \nu_3\sigma_3$, and the theoretical curve corresponded well with the measured curve.

ACKNOWLEDGMENTS

We gratefully acknowledge the financial support for this work provided by National project funding for Key R&D programs of China

(2022YFC3004702) and National Natural Science Foundation of China (52074276).

DECLARATIONS

Conflict of Interest The authors declare that there is no conflict of interest regarding the publication of this paper.

REFERENCES

- Du, W. G., Chai, J., Zhang, D. D., & Lei, W. L. (2021). Application of optical fiber sensing technology in similar model test of Shallow-buried and thick coal seam mining. *Measurement*, *181*, 109559.
- Du, H. B., Dai, F., Li, A., & Jiang, R. C. (2023). Dynamic responses and failure behaviors of saturated rocks subjected to repetitive compression-shear impacting. *Rock Mechanics and Rock Engineering*, *56*(7), 4697–4714.
- Feng, J. J., Wang, E. Y., Chen, L., Li, X. L., Xu, Z. Y., & Li, G. A. (2016). Experimental study of the stress effect on attenuation of normally incident P-wave through coal. *Journal of Applied Geophysics*, *132*, 25–32.
- Feng, P., Xu, Y., & Dai, F. (2021). Effects of dynamic strain rate on the energy dissipation and fragment characteristics of cross-fissured rocks. *International Journal of Rock Mechanics and Mining Sciences*, *138*, 104600.
- Gong, H. L., Luo, Y., Zhou, J. R., Zhao, C. C., & Li, X. P. (2023). Fracture behaviors and damage evolution anisotropy of granite under coupling of multiaxial confinement and dynamic loading. *Rock Mechanics and Rock Engineering*, *56*(4), 2515–2534.
- Gu, Z. J., Shen, R. X., Liu, Z. T., Zhao, E. L., Chen, H. L., Yuan, Z. C., & Tian, J. W. (2023a). Dynamic characteristics of coal under triaxial constraints based on the split-Hopkinson pressure bar test system. *Natural Resources Research*, *32*, 587–601.
- Gu, Z., Shen, R., Liu, Z., Zhou, X., Li, X., Zang, Z., & Wang, X. (2023b). Strain rate effect and mechanical constitutive model

- of coal samples under dynamic load. *Natural Resources Research*, 32(6), 2769–2785.
- Han, Z. Y., Li, D. Y., Zhou, T., Zhu, Q. Q., & Ranjith, P. G. (2020). Experimental study of stress wave propagation and energy characteristics across rock specimens containing cemented mortar joint with various thicknesses. *International Journal of Rock Mechanics and Mining Sciences*, 131, 104352.
- Han, Z. Y., Li, D. Y., & Li, X. B. (2022). Dynamic mechanical properties and wave propagation of composite rock-mortar specimens based on SHPB tests. *International Journal of Mining Science and Technology*, 32(4), 793–806.
- Hu, J., He, M. C., Li, H. R., Tao, Z. G., Liu, D. Q., Cheng, T., & Peng, D. (2024). Rockburst hazard control using the excavation compensation method (ECM): A case study in the Qinling water conveyance tunnel. *Engineering*, 34, 154–163. <https://doi.org/10.1016/j.eng.2023.11.013>.
- Huang, J., Liu, X. L., Zhao, J., Wang, E. Z., & Wang, S. J. (2020). Propagation of stress waves through fully saturated rock joint under undrained conditions and dynamic response characteristics of filling liquid. *Rock Mechanics and Rock Engineering*, 53(8), 3637–3655.
- Jin, J. F., Yuan, W., Wu, Y., & Guo, Z. Q. (2020). Effects of axial static stress on stress wave propagation in rock considering porosity compaction and damage evolution. *Journal of Central South University*, 27(2), 592–607.
- Ju, Y., Sudak, L., & Xie, H. P. (2007). Study on stress wave propagation in fractured rocks with fractal joint surfaces. *International Journal of Solids and Structures*, 44(13), 4256–4271.
- Kong, X. G., Li, S. G., Wang, E. Y., Ji, P. F., Wang, X., Shuang, H. Q., & Zhou, Y. X. (2021). Dynamics behaviour of gas-bearing coal subjected to SHPB tests. *Composite Structures*, 256, 113088.
- Li, Y. X., Zhu, Z. M., Li, B. X., Deng, J. H., & Xie, H. P. (2011). Study on the transmission and reflection of stress waves across joints. *International Journal of Rock Mechanics and Mining Sciences*, 48(3), 364–371.
- Li, D. Y., Han, Z. Y., Zhu, Q. Q., Zhang, Y., & Ranjith, P. G. (2019). Stress wave propagation and dynamic behavior of red sandstone with single bonded planar joint at various angles. *International Journal of Rock Mechanics and Mining Sciences*, 117, 162–170.
- Li, B. L., Wang, E. Y., Hu, S. B., Wang, X. F., & Liu, B. (2021). A study of vibration velocity attenuation induced by pneumatic rock breaking with carbon dioxide ice powder for safety assessment. *Rock Mechanics and Rock Engineering*, 54(12), 6481–6493.
- Li, B. L., Wang, E. Y., Li, Z. H., Cao, X., Liu, X. F., & Zhang, M. (2023a). Automatic recognition of effective and interference signals based on machine learning: A case study of acoustic emission and electromagnetic radiation. *International Journal of Rock Mechanics and Mining Sciences*, 170, 105505.
- Li, H. R., He, M. C., Qiao, Y. F., Cheng, T., Xiao, Y. M., & Gu, Z. J. (2023b). Mode I fracture properties and energy partitioning of sandstone under coupled static-dynamic loading: Implications for rockburst. *Theoretical and Applied Fracture Mechanics*, 127, 104025.
- Li, H. R., Qiao, Y. F., He, M. C., Shen, R. X., Gu, Z. J., Cheng, T., & Tang, J. (2023c). Effect of water saturation on dynamic behavior of sandstone after wetting-drying cycles. *Engineering Geology*, 319, 107105.
- Li, X. L., Liu, Z. T., Zhao, E. L., Liu, Y. B., Feng, X. J., & Gu, Z. J. (2023d). Experimental study on the damage evolution behavior of coal under dynamic brazilian splitting tests based on the split hopkinson pressure bar and the digital image correlation. *Natural Resources Research*, 32(3), 1435–1457.
- Li, X. L., Zhao, E. L., Liu, Z. T., Liu, Y. B., Feng, X. J., & Gu, Z. J. (2023e). Experimental study on multiple propagation characteristics of stress wave and surface displacement behavior in coal based on SHPB and DIC. *Bulletin of Engineering Geology and the Environment*, 82(7), 246.
- Liu, K., Zhang, Q. B., Wu, G., Li, J. C., & Zhao, J. (2019). Dynamic Mechanical and fracture behaviour of sandstone under multiaxial loads using a triaxial Hopkinson bar. *Rock Mechanics and Rock Engineering*, 52(7), 2175–2195.
- Liu, X. F., Zhang, S. Q., Wang, E. Y., Zhang, Z. B., Wang, Y., & Yang, S. L. (2023). Multi-Index geophysical monitoring and early warning for rockburst in coalmine: A case study. *International Journal of Environmental Research and Public Health*, 20(1), 392.
- Liu, X. F., Cai, D. K., Gu, Z. I., Zhang, S. Q., Zhou, X., & Gao, A. (2024). Analysis of progressive damage and energy consumption characteristics of gas-bearing coal under cyclic dynamic loads. *Energy*, 306, 132419. <https://doi.org/10.1016/j.energy.2024.132419>.
- Luo, Y., Gong, H. L., Huang, J. H., Wang, G., Li, X. P., & Wan, S. (2022). Dynamic cumulative damage characteristics of deep-buried granite from Shuangjiangkou hydropower station under true triaxial constraint. *International Journal of Impact Engineering*, 165, 104215.
- Niu, L. L., Zhu, W. C., Li, S., & Liu, X. G. (2020). Spalling of a one-dimensional viscoelastic bar induced by stress wave propagation. *International Journal of Rock Mechanics and Mining Sciences*, 131, 104317.
- Shen, R., Hou, Z., Yuan, Z., Li, Y., & Gu, Y. (2024). Development of a three-dimensional stress monitoring system for coal rock and its application in a mine. *Rock Mechanics and Rock Engineering*, 57(3), 1983–1996. <https://doi.org/10.1007/s00603-023-03661-0>.
- Shen, R. X., Gu, Z. J., Liu, Z. T., Zhao, E. L., Zang, Z. S., Zhou, X., & Wang, X. (2023). Study on impact dynamic behavior and failure characteristics of coal based on true triaxial split-Hopkinson pressure bar experiments. *Natural Resources Research*, 32(6), 2845–2866.
- Tan, T. J., Wang, E. Y., Wang, X. R., & Yao, W. L. (2023). Study on the electrical impedance response and conductivity mechanism of coal mass rupture under impact load. *Measurement*, 219, 113164.
- Wang, X. H., Zhang, S. R., Wang, C., Shang, C., Cao, K. L., & Wei, P. Y. (2018). Investigation into stress wave propagation across interlayers existing in roller compacted concrete (RCC) under impact loadings. *Construction and Building Materials*, 193, 13–22.
- Wang, L. J., Fan, L. F., & Du, X. L. (2022a). Non-attenuation behavior of stress wave propagation through a rock mass. *Rock Mechanics and Rock Engineering*, 55(7), 3807–3815.
- Wang, J., Ma, L., Zhao, F., Lv, B. G., Gong, W. L., He, M. C., & Liu, P. (2022b). Dynamic strain field for granite specimen under SHPB impact tests based on stress wave propagation. *Underground Space*, 7(5), 767–785.
- Wang, X. F., Hu, S. B., Wang, E. Y., Zhang, Q., & Liu, B. (2023). Experimental research and energy analysis of a new type of dry ice powder pneumatic rock breaking technology. *International Journal of Mining Science and Technology*, 33(4), 423–435.
- Xie, H., Liu, X. F., Zhang, H. J., Wang, E. Y., Li, X. L., & Lu, J. J. (2022a). Internal strain monitoring of coal samples based on fiber Bragg grating sensing. *Measurement*, 187, 110335.
- Xie, H. P., Lu, J., Li, C. B., Li, M. H., & Gao, M. Z. (2022b). Experimental study on the mechanical and failure behaviors of deep rock subjected to true triaxial stress: A review. *International Journal of Mining Science and Technology*, 32(5), 915–950.
- Yan, Z. L., Dai, F., Zhu, J. B., & Xu, Y. (2021). Dynamic cracking behaviors and energy evolution of multi-flawed rocks under static pre-compression. *Rock Mechanics and Rock Engineering*, 54(9), 5117–5139.

Deformation Characteristics and Mechanical Constitutive Model

- Yang, Q., Wang, M., Zhao, X., & Fan, L. F. (2023). Experimental study of frequency-temperature coupling effects on wave propagation through granite. *International Journal of Rock Mechanics and Mining Sciences*, *162*, 105326.
- Yu, X., Chen, L., Fang, Q., Zhang, J. H., Guo, D., & Hou, X. F. (2019). Determination of attenuation effects of coral sand on the propagation of impact-induced stress wave. *International Journal of Impact Engineering*, *125*, 63–82.
- Zang, Z. S., Li, Z. H., Gu, Z. J., Niu, Y., Yin, S., Kong, X. G., & Zhang, X. (2024a). The multi-dimensional joint response of the electric potential time-frequency-field in the fracture process of flawed coal under dynamic load. *Theoretical and Applied Fracture Mechanics*, *131*, 104415.
- Zang, Z. S., Li, Z. H., Zhang, X., Kong, X. G., Gu, Z. J., Yin, S., & Niu, Y. (2024b). Electric potential response characteristics of coal under stress wave loading. *Natural Resources Research*, *33*(3), 1289–1307.
- Zang, Z. S., Li, Z. H., Niu, Y., & Yin, S. (2024c). Experimental investigation of the fracture and damage evolution characteristics of flawed coal based on electric potential and acoustic emission parameter analyses. *Engineering Fracture Mechanics*, *295*, 109740. <https://doi.org/10.1016/j.engfracmec.2023.109740>.
- Zhang, S. Q., Liu, X. F., Zhang, H. J., Piao, C. D., & Niu, Y. (2023). Study on the Force Model of Squeezed Branch Piles Based on Surface Potential Characteristics. *Buildings*, *13*(9), 2231.
- Zhang, L., Wang, E. Y., Liu, Y. B., Yue, W. T., & Chen, D. (2024). Experimental research into the dynamic damage characteristics and failure behavior of rock subjected to incremental repeated impact loads. *Engineering Geology*, *331*, 107435.
- Zhou, X., Liu, X. F., Wang, X. R., Liu, Y. B., Xie, H., & Du, P. F. (2023a). Acoustic emission characteristics of coal failure under triaxial loading and unloading disturbance. *Rock Mechanics and Rock Engineering*, *56*(2), 1043–1061.
- Zhou, X., Liu, X. F., Wang, X. R., Xie, H., & Du, P. F. (2023b). Failure characteristics and mechanism of coal under the coupling between different confining pressures and disturbance loading. *Bulletin of Engineering Geology and the Environment*, *82*(12), 442.
- Wang, D., Wang, E., Liu, X., Feng, X., Wei, M., Li D., Li, B., Liu, Q., Zhang, X., Yang, H., & Guo C. (2024). Non-linear response of acoustic emission and electric potential during creep failure of coal under stepwise increasing loads: Insights from multifractal theory. *Natural Resources Research*. <http://doi.org/10.1007/s11053-024-10366-w>.

Springer Nature or its licensor (e.g. a society or other partner) holds exclusive rights to this article under a publishing agreement with the author(s) or other rightsholder(s); author self-archiving of the accepted manuscript version of this article is solely governed by the terms of such publishing agreement and applicable law.